Layout: T1 Standard SC | Book ID: 272293_1_En | Book ISBN: 978-3-642-40153-4
Chapter No.: 18 | Date: 17-8-2013 | Page: 1/23

Author Proof

Chapter 18
Use of Receding Horizon Optimal Control to Solve MaxEP-based Biogeochemistry Problems

Joseph J. Vallino, Christopher K. Algar, Nuria Fernández González and Julie A. Huber

Abstract The maximum entropy production (MaxEP) principle has been applied to steady state systems, but biogeochemical problems of interest are typically transient in nature. To apply MaxEP to biogeochemical reaction networks, we propose that living systems maximum entropy production over appropriate time horizons based on strategic information stored in their genomes, which differentiates them from inanimate chemistry, such as fire, that maximizes entropy production instantaneously. We develop a receding horizon optimal control procedure that maximizes internal entropy production over different intervals of time. This procedure involves optimizing the stoichiometry of a reaction network to determine how biological structure is partitioned to reactions over an interval of time. The modeling work is compared to a methanotrophic microcosm experiment that is being conducted to examine how microbial systems integrate entropy production over time when subject to time varying energy input attained by periodically cycling feed-gas composition. The MaxEP-based model agrees well with experimental results, and model analysis shows that increasing the optimization time horizon increases internal entropy production.

Accepted (July 2012) in: *Beyond the Second Law: Entropy Production and Non-Equilibrium Systems*. R. C. Dewar, C. H. Lineweaver, R. K. Niven and K. Regenauer-Lieb, Springer.

18.1 Introduction

In this chapter we examine the application of the maximum entropy production (MaxEP) principle for describing microbial biogeochemistry. Biogeochemistry enlists the fields of biology and geochemistry to understand chemical transformations and element cycling that occur in natural environments. Because the

J. J. Vallino (✉) · C. K. Algar · N. F. González · J. A. Huber
Marine Biological Laboratory, Woods Hole, MA, USA
e-mail: jvallino@mbl.edu

R. C. Dewar et al. (eds.), *Beyond the Second Law*,
Understanding Complex Systems, DOI: 10.1007/978-3-642-40154-1_18,
© Springer-Verlag Berlin Heidelberg 2014

UNCORRECTED PROOF

Layout: T1 Standard SC | Book ID: 272293_1_En | Book ISBN: 978-3-642-40153-4
Chapter No.: 18 | Date: 17-8-2013 | Page: 2/23

Author Proof

majority of biologically catalyzed reactions that occur on Earth, such as nitrogen fixation, denitrification, metal redox reactions, sulfate reduction, etc., are orchestrated by bacteria and archaea [12], we restrict our current focus to microbially catalyzed reactions. Microbes (including viruses, bacteria and archaea) are the simplest living organisms and are at the interface between chemistry and biology because they catalyzed reactions that also occur abiotically, such as the oxidation of iron (rusting), oxidation of hydrogen sulfide and methane, fixing N_2 into NH_3 and HNO_3 (lightening and combustion). Since we can view bacteria and archaea as simple molecular machines [12], they are most likely amendable to thermodynamic description. They are critical for the support and functioning of all higher life on Earth, so it is particularly important to understand how their presence and growth controls the chemistry at local, regional and global scales. Our expectation is that by employing MaxEP we will be able to develop more robust models that can be used to study how biogeochemistry changes as the environment is altered by natural phenomena and human actions.

Biogeochemistry can be viewed from two extreme perspectives. In the classic perspective, organisms determine the overall biogeochemical processes that occur in an ecosystem. This organismal centric view derives naturally from reductionism, as biogeochemistry is by definition a product of organismal growth. However, the organismal centric view implies that changing species composition will likely produce different biogeochemistry. Furthermore, this approach requires detailed knowledge on organism growth kinetics, predator–prey interactions, as well as on how community composition may change as a result of internal dynamics or external drivers. Except for extremely simple systems, this information is usually lacking. Despite these short comings, the majority of biogeochemical models use the organismal perspective as a basis of their design [13].

The second perspective on biogeochemistry takes a systems approach and views ecosystems thermodynamically as open, non-equilibrium systems. In this case, it is free energy potential, resource availability and information that determine ecosystem biogeochemistry. While organisms ultimately carry out the process, thermodynamics determines which metabolic functions will dominate. Organisms are viewed as interchangeable components, similar to microstates that underlie macrostates in equilibrium thermodynamics [44]. It is this thermodynamic perspective that we will employ to describe ecosystem biogeochemistry, where MaxEP will serve as the governing principle. Because we will limit our analysis to microbial processes, we will remove the typical organismal emphasis and instead view a microbial community in functional terms as a collection of catalysts (or molecular machines [12]) that are synthesized and degraded to achieve MaxEP.

In this chapter we develop a MaxEP-based biogeochemical (BGC) model of a distributed metabolic network. Model degrees of freedom are determined by solving a receding horizon optimal control problem that maximizes entropy production over successive intervals of time. Results from the model are compared to data from two methanotrophic microcosm experiments, a control, and a treatment where energy input is cycled over a 20 day period.

UNCORRECTED PROOF

Layout: T1 Standard SC | Book ID: 272293_1_En | Book ISBN: 978-3-642-40153-4
Chapter No.: 18 | Date: 17-8-2013 | Page: 3/23

Author Proof

18.2 MaxEP and Living Systems

The MaxEP conjecture [8, 10, 35, 36] states that steady state, non-equilibrium systems with many degrees of freedom will likely be found in a state that maximizes internal entropy production. If internal self-organization, such as vortices and macroscopic structures, facilitates internal entropy production, then those structures will likely develop [26]. Similar to equilibrium thermodynamics that requires systems to be found in the state of maximum entropy, MaxEP indicates that nonequilibrium systems will head towards equilibrium along the fastest possible pathway. That is, they will dissipate free energy as fast as possible within the constraints imposed on the system [28, 44]. As discussed in this book and elsewhere, several phenomena appear consistent with MaxEP, including planetary-scale heat transport [19, 27], laminar to turbulent flow transition [29], plant evapotranspiration [46], and many others (see [35] and references therein).

18.2.1 Living Systems as Catalysts

If MaxEP indicates that systems should race down free energy surfaces towards equilibrium as fast as possible, then why isn't the universe already at equilibrium? The answer is because systems often get trapped in metastable states. For instance, a mixture of methane and air at 20 °C, even within the combustible mixture envelope (5–15 % CH_4), will remain in this metastable state for a considerable length of time due to the high activation energy required to overcome the repulsive force of the electron cloud that prevents spontaneous reaction. Of course, if a spark is introduce, then the highly exothermic reaction proceeds in a MaxEP manner due to the increase in temperature. Another means in which the free energy can be released is by introducing a catalyst. By reducing the activation energy, the catalyst frees the system from its metastable state, so the reaction can proceed at room temperature even if the system lies outside the combustion envelope or the reactants are dissolved in water.

While most man-made catalysis are crude and exhibit poor selectivity, enzyme catalysts synthesized by bacteria, as well as all living organisms, achieve extreme reductions in activation energies along very selective reaction pathways. It is the presence of these enzyme catalysts that hastens the dissipation of free energy and entropy production through the destruction of chemical and electromagnetic potentials. However, the increase in reaction rates provided by catalysts is proportional to the amount of catalyst present. To maximize entropy production, it is necessary for a system to rely on autocatalytic reactions that not only dissipate chemical potential but also synthesize more catalyst in the process, such as the methane oxidation reaction given by,

UNCORRECTED PROOF

Layout: T1 Standard SC | Book ID: 272293_1_En | Book ISBN: 978-3-642-40153-4
Chapter No.: 18 | Date: 17-8-2013 | Page: 4/23

Author Proof

$$CH_4 + 2O_2 + \Sigma \xrightarrow{\mathbb{S}} \mathbb{S} + H_2CO_3 + H_2O \tag{18.1}$$

where $\mathbb{S}$ is a catalyst, or *biological structure*, synthesized from available resources, such as C, N, P, Fe, in the environment, Σ. Because catalyst is produced as a product of methane oxidation in Eq. (18.1), the reaction will proceed exponentially provided resources, Σ, needed to build catalyst are not limiting. Of course, Eq. (18.1) also represents growth of methanotrophs (specialized bacteria that eat methane), but we are placing emphasis here on catalyst synthesis for the dissipation of chemical potential, not on the nature of bacterial growth. This distinction *represents a paradigm shift from 'we eat food' to 'food has produced us to eat it'* [25].

In order to calculate the rate of en action, Eq. (18.1), we need to know the standard molar entropy associated with biological structure, $\mathbb{S}$. Unfortunately, there is considerable confusion associated with entropy calculations involving living organisms. It is often believed that living organisms represent extremely low entropy structures. This misconception can be attributed to confusion over the association between entropy and order. Order, as might be represented by a pattern, does contribute to entropy, but the entropy (or free energy) of the material the pattern is constructed from must also be accounted for in the entropy calculation. As [34] has shown, only when the pattern is written at the atomic scale does the entropy of the pattern become significant compared to the entropy of the material the pattern is written in.

Consider the words written on this page. Because the ink on the page forms a pattern that contains information, the entropy of the page is lower than a page with randomized letters [5]; however, the reduction of entropy is trivial compared to the entropy of the paper the ink is written on. If the paper is burned, it hardly matters in a thermodynamic context if the text contains the meaning of life or only jibberish; the difference in the amount of free energy dissipated, or entropy produced, between the two cases is virtually undetectable, because the pattern on this page is written at a macroscopic scale. Likewise, entropy associated with information contained in DNA/RNA or protein is small compared to the entropy associated with the nucleic or amino acid polymers the information is written in [45]. All too often the entropy of the material a pattern is written in is overlooked, which leads to incorrect assessments, such as the popular statement that a clean desk has lower entropy than a messy one; both have the same thermodynamic entropy or free energy. In terms of entropy and free energy calculations, a gram of freeze-dried yeast or bacteria, which are viable upon rehydration, has the same molar entropy and free energy of formation as an equivalent weight of a macromolecules in the appropriate proportions [3]. To paraphrase [34], the *élan vital* carries no thermodynamic burden.

While the entropy associated with the information content of a cell is trivial compared to the material of a cell, it is nevertheless of critical importance. It is

UNCORRECTED PROOF

Layout: T1 Standard SC | Book ID: 272293_1_En | Book ISBN: 978-3-642-40153-4
Chapter No.: 18 | Date: 17-8-2013 | Page: 5/23

Author Proof

useful information [1] contained in the genome that allows for the construction of complex macromolecules that gives rise to the catalytic nature of biological structure, $\mathcal{S}$. Ultimately, then, it is information that releases systems from metastable states to flow down free energy surfaces and produce entropy. Evolution works to refine this information and thereby increase the rate of entropy production. Information and entropy are intimately coupled [17]. Philosophically, we postulate free energy spawns the creation of information that hastens free energy's destruction.

18.2.2 MaxEP and Transient Systems

An element of time has been implied in the MaxEP description above for constructing biological structure to dissipate free energy; however, all MaxEP theories to date have been applied to steady state systems only, where time is not involved in the equations. There currently does not exist a MaxEP theory for transient systems where the state is allowed to vary with time, but it is transient systems we are often most interested in. The objective in modeling is usually to understand and predict how a system of interest will respond to perturbations or changes in external drivers. To build a transient biogeochemistry model based on MaxEP requires that we speculate as to how time may affect the MaxEP solution.

For any particular system we can define internal entropy production once the system boundaries have been defined [32, 35], as well as formulate an entropy balance equation, such as

$$\frac{dS}{dt} = J_S + \dot{\sigma} \tag{18.2}$$

where S is system entropy (kJ K^{-1}), J_S is the entropy flux into the system (from mass and heat transport) and $\dot{\sigma}$ is the entropy production rate due to irreversible processes occurring within the system. The second law requires that $\dot{\sigma} \geq 0$ [20]. We also define σ as $\int \dot{\sigma} dt$, which is the amount entropy that derives from internal irreversible processes over some interval of time. Throughout this manuscript we will only be concerned with σ or $\dot{\sigma}$, but not S, because MaxEP applies to internal entropy production only.

For a transient system, internal entropy production is a function of time, $\dot{\sigma}(t)$, so how can MaxEP be defined when $\dot{\sigma}$ varies with time? One special case would be to maximize $\dot{\sigma}$ at every instance in time, which would be equivalent to taking a steepest decent pathway along the free energy surface defined by the current state and all possible pathways leading from that point, similar to water flowing downhill. However, following a steepest decent pathway at each instance in time may not lead to the greatest internal entropy production over an interval of time. Consider Fig. 18.1 for example. Instantaneous internal entropy production at time t_n is greater along pathway PA than along pathway PB, since $\dot{\sigma}_A(t_n) > \dot{\sigma}_B(t_n)$. But taking the

UNCORRECTED PROOF

Layout: T1 Standard SC | Book ID: 272293_1_En | Book ISBN: 978-3-642-40153-4
Chapter No.: 18 | Date: 17-8-2013 | Page: 6/23

Author Proof

B & W IN PRINT

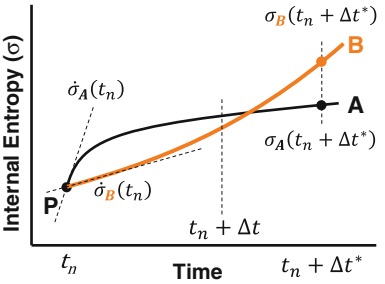

Fig. 18.1 Increases in internal entropy over two possible pathways starting from point P at time t_n. Here, σ is the part of system entropy S that is from internal irreversible processes and $\dot{\sigma}$ its production rate

steepest descent pathway at point P sets the system along a trajectory that ultimately produces less internal entropy than had the system followed pathway PB, since $\sigma_B(t_n + \Delta t^*) > \sigma_A(t_n + \Delta t^*)$. If the system had a means to explore all possible future pathways leading from P over Δt^* time, then the system could increase entropy produced over the steepest descent pathway, PA, by following pathway PB. That is, if the system has a way to generate predictions, then forgoing the steepest descent pathway can lead to greater internal entropy production over time. We postulate that this is precisely what living systems do.

Because living systems can store information in their genome, they can develop temporal strategies based on passed events that become refined via evolutionary selection. Genomic information not only allows organisms to access free energy trapped in metastable states, but also allows them to follow pathways that avoid the steepest decent route and produce more entropy over time. For instance, some bacteria form spores or dormant cells that increase their fitness when conditions become hostile [23, 24]. Likewise, many organisms will increase fat storage in the fall to survive the winter months. While temporal strategies are well recognized, they are often not accounted for in models. Instead, most biogeochemistry models view the system as a type of Markov process where system response only depends on the current state. We believe what differentiates abiotic systems from biotic ones, is the ability of the latter to store information that allows them to develop temporal strategies and out compete abiotic systems over time in internal entropy production [44]. Maximizing internal entropy produced over intervals of time is the basis of the model and associated experiment discussed in the next section.

18.3 Methods

Discussed below are descriptions of a microbial microcosm experiment and an associated mathematical model that are intended to explore the idea that living systems develop temporal strategies that increase entropy production when averaged over time. The experimental setup employs methanotrophic microcosms whose energy input is cycled over time, while the modeling of the microcosms is based on a distributed metabolic network of biochemical reactions that are

UNCORRECTED PROOF

Layout: T1 Standard SC | Book ID: 272293_1_En | Book ISBN: 978-3-642-40153-4
Chapter No.: 18 | Date: 17-8-2013 | Page: 7/23

Author Proof

controlled to maximize averaged entropy production over intervals of time using a receding horizon optimal control approach.

18.3.1 Experimental System

The experiment is designed to examine how microbial communities adapt and evolve to cope with periodic energy inputs using methane plus air as the sole source of energy. The experimental setup [44] consists of four 18 L microcosms that are operated in chemostat mode at a dilution rate of 0.1 d^{-1} and are sparged at a gas flow rate of 20 mL min^{-1} (0 °C, 101.3 kPa). Two control microcosms are sparged continuously with a gas mixture of 4.9 % CH_4, 19.6 % O_2, 0.03 % CO_2, balance N_2, while two other microcosms are cycled between the methane plus air mixture and just air (20.95 % O_2, 0.033 % CO_2, balance N_2) over a 20 d period (10 days with CH_4 on, 10 days with CH_4 off). All microcosms were inoculated approximately 4 years ago with whole water samples collected from a coastal pond and cedar bog (1 L each). A mineral salts medium (10 mM K_2HPO_4, 50 μM KNO_3, 100 μM $MgSO_4$, 100 μM $CaCl_2$, 100 μM NaCl, plus trace elements solution) adjusted to pH 6.8 is used as feed.

Output gas composition is analyzed on-line every 5 h for CH_4 (NDIR, California Analytical Instruments), O_2 and CO_2 (laser diode adsorption spectroscopy, Oxigraf) concentrations, and analyzer drift is compensated for by monitoring input gas composition. Dissolved oxygen and pH electrodes are measured and recorded every hour. Gas cycling and all data acquisition are under computer control and posted on-line (http://ecosystems.mbl.edu/MEP). Periodically, liquid samples are withdrawn for both nutrient analysis (NO_3^-, NH_3, particulate organic C (POC), N (PON), dissolved organic C (DOC), and N (DON)) and microbial community assessment via cell counts and 454-tag pyrosequencing of the V4-V6 hypervariable regions of the 16S rRNA gene [16].

18.3.2 Metabolic Network Model

The MaxEP-based biogeochemistry model uses a distributed metabolic network approach to simulate the functional attributes of a microbial community [43]. For the methanotrophic microcosms, four biological structures are used to capture methane oxidation to methanol $\mathbb{S}_1$, methanol to CO_2 $\mathbb{S}_2$, the turnover of biological structures $\mathbb{S}_3$, and the consumption of recalcitrant (i.e., hard to decompose) organic C (dC) and N (dN), $\mathbb{S}_4$ (Table 18.1 and Fig. 18.2). This metabolic network structure differs significantly from our previous approach [44]. Here, we use whole reactions instead of half reactions to represent metabolism, which has two main advantages: (1) since half reactions produce (or consume) electrons, we do not need equations and constraints to insure electron conservation and (2) biological

UNCORRECTED PROOF

Layout: T1 Standard SC | Book ID: 272293_1_En | Book ISBN: 978-3-642-40153-4
Chapter No.: 18 | Date: 17-8-2013 | Page: 8/23

Author Proof

Table 18.1 Reaction stoichiometries and optimal control variables (*OCV*: ε_j and $\omega_{i,j}$ in Eq. 18.4) associated with the four biological structures used to represent methanotrophic communities

Reaction Rate	Stoichiometry	OCV
$r_{1,1}$	$CH_4 + \varepsilon_1\gamma_1 HNO_3 + a_{1,1}O_2 \xrightarrow{\mathbb{S}_1} \varepsilon_1\mathbb{S}_1 + (1-\varepsilon_1)CH_3OH + b_{1,1}H_2O$	$\varepsilon_1, \omega_{1,1}$
$r_{2,1}$	$CH_4 + \varepsilon_1\gamma_1 NH_3 + a_{2,1}O_2 \xrightarrow{\mathbb{S}_1} \varepsilon_1\mathbb{S}_1 + (1-\varepsilon_1)CH_3OH + b_{2,1}H_2O$	
$r_{1,2}$	$CH_3OH + \varepsilon_2\gamma_2 HNO_3 + a_{1,2}O_2 \xrightarrow{\mathbb{S}_2} \varepsilon_2\mathbb{S}_2 + (1-\varepsilon_2)H_2CO_3 + b_{1,2}H_2O$	$\varepsilon_2, \omega_{1,2}$
$r_{2,2}$	$CH_3OH + \varepsilon_2\gamma_2 NH_3 + a_{2,2}O_2 \xrightarrow{\mathbb{S}_2} \varepsilon_2\mathbb{S}_2 + (1-\varepsilon_2)H_2CO_3 + b_{2,2}H_2O$	
$r_{i,3}$	$\mathbb{S}_i + a_{i,3}O_2 \xrightarrow{\mathbb{S}_3} \varepsilon_3\mathbb{S}_3 + (1-\varepsilon_3)\left[\gamma_i(\varepsilon_3 NH_3 + (1-\varepsilon_3)\mathrm{dN}) + \varepsilon_3 H_2CO_3 + (1-\varepsilon_3)\mathrm{dC}\right] + \varepsilon_3(\gamma_i - \gamma_3)NH_3 + b_{i,3}H_2O \quad \text{for } i = 1,\ldots,4$	ε_3
$r_{1,4}$	$dCN + a_{1,4}O_2 \xrightarrow{\mathbb{S}_4} \varepsilon_4\mathbb{S}_4 + (1-\varepsilon_4)H_2CO_3 + b_{1,4}H_2O + d_{1,4}NH_3$	ε_4

Biological structure is unit carbon based and its composition is given by $CH_{\alpha_j}O_{\beta_j}N_{\gamma_j}$. The stoichiometric coefficients, $a_{i,j}$, $b_{i,j}$ and $d_{1,4}$ are determined from O, H and N elemental balances for each reaction as necessary

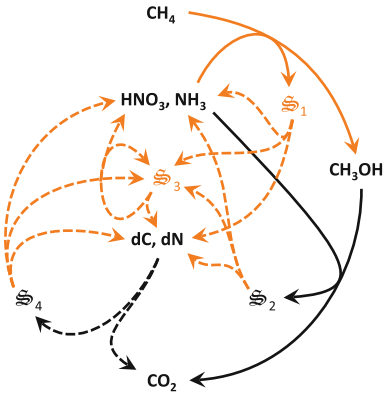

Fig. 18.2 Distributed reaction network for methanotrophic communities. dC and dN: recalcitrant organic C and N, respectively. Lines of similar color and style represent a single reaction group. H_2CO_3 not shown to improve readability. See Table 18.1 for stoichiometry

B & W IN PRINT

UNCORRECTED PROOF

structure synthesis is directly coupled to its associated redox reaction pair. Nevertheless, networks based on half reactions are useful for discovering important reaction pairs that evade detection, such as anammox [21], because models based on half reactions build their own redox pair combinations.

Reaction stoichiometries are parameterized by two types of optimal control variables, ε_j and $\omega_{i,j}$, where the former controls the efficiency of biological structure synthesis, and the latter controls how biological structure is allocated to

Layout: T1 Standard SC | Book ID: 272293_1_En | Book ISBN: 978-3-642-40153-4
Chapter No.: 18 | Date: 17-8-2013 | Page: 9/23

Author Proof

sub-reactions associated with each biological structure (Table 18.1). For instance, $\omega_{1,1}$ determines how $\mathfrak{S}_1$ is partitioned between nitrate uptake ($r_{1,1}$) and ammonia uptake ($r_{2,1}$). The value of ε_j plays a critical role in the model, because as ε_j approaches 0 the reaction behaves as pure combustion dissipating substantial amounts of free energy, while as ε_j approaches 1 biological structure is synthesized with minimum free energy dissipation and maximum conversation of C substrate into biomass. As discussed above and elsewhere [45], reaction free energy for biological structure synthesis as ε_j approaches 1 is still negative or within the neighborhood of 0, but in order to achieve a growth efficiency of near 100 %, reactions must proceed reversibly (i.e., infinitely slowly). This thermodynamic constraint explains why we do not find bacteria opting for an ε_j near 1 strategy.

The partitioning of labile (i.e., easily degraded) versus detrital C and N in the four reactions associated with biological structure decomposition, $r_{i,3}$, is solely determined by ε_3. While this is a crude approximation, it has the advantage that no additional parameters are needed. One of the objectives of the model is to limit the number of adjustable parameters and place as many degrees of freedom as possible in the optimal control variables ε_j and $\omega_{i,j}$. The detrital C (dC) and N (dN) pools are modeled separately, but are treated as a single molecule, dCN, in reaction $r_{1,4}$ with its concentration, c_{dCN}, set to c_{dC} and its N:C ratio given by $\gamma_{\mathrm{dCN}} = c_{\mathrm{dN}}/c_{\mathrm{dC}}$.

Total internal entropy produced by the microbial community (kJ K^{-1}), ignoring small contributions from mixing entropy [45], is readily calculated from the product of reaction rate ($r_{i,j}$) and the associated reaction free energy ($\Delta_r G_{r_{i,j}}$) summed over each reaction in the network, as given by,

$$\dot{\sigma}(t) = -\frac{V_L}{T}\sum_{j=1}^{n_S}\sum_{i=1}^{n_{Sj}} r_{i,j}(t)\Delta_r G_{r_{i,j}}(t) \tag{18.3}$$

where V_L is the liquid volume of the microcosms (m^3), T is temperature (K), n_S is the number of biological structures (4 in this case), and n_{S_j} is the number of sub-reactions associate with $\mathfrak{S}_j$ (Table 18.1). We use [2] approach for calculating reaction free energies, $\Delta_r G_{r_{i,j}}$, that accounts for species concentrations and activity coefficients, and [4] value for the free energy of formation of biological structure (see also [44, 45]).

Reaction rates are given by the following modified Monod kinetics expression [45]

$$r_{i,j} = v_j\varepsilon_j^2(1-\varepsilon_j^2)\prod_{k=1}^{n_c}\left(\frac{c_k}{c_k+\kappa_j\varepsilon_j^4}\right)^{\Lambda_{i,j,k}}\omega_{i-1,j}\prod_{l=i}^{n_{S_j}-1}(1-\omega_{l,j})f_G(\Delta_r G_{r_{i,j}})c_{S_j}. \tag{18.4}$$

The parameters v_j and κ_j were chosen to capture bacterial growth kinetics observed in nutrient deplete (i.e., oligotrophic) to nutrient abundant (i.e., eutrophic) conditions. That is, v_j and κ_j are independent of community composition. The exponent $\Lambda_{i,j,k}$ is set to either 0 or 1 depending on reaction stoichiometry (Table 18.1) for the n_c state concentration variables, c_k, and $\omega_{l,j}$ determines how

UNCORRECTED PROOF

Author Proof

$\mathbb{S}_j$ is partitioned to its associated n_{S_j} sub-reactions, where $\omega_{0,j} = 1$ for all reactions. For all model runs, we assume decomposition of biological structure occurs indiscriminately, so that $\omega_{i,3} = c_{S_{i+1}} / \sum_{k=1}^{i+1} c_{S_k}$ for $i = 1, \ldots, 4$. To insure no reaction proceeds if its free energy of reaction, $\Delta_r G_{r_{i,j}}$, is greater than zero, the function f_G is set to,

$$f_G(\Delta_r G_{r_{i,j}}) = \begin{cases} 1 - e^{\chi_G \Delta_r G_{r_{i,j}}} & \Delta_r G_{r_{i,j}} \le 0 \\ 0 & \Delta_r G_{r_{i,j}} > 0 \end{cases} \quad ; \tag{18.5}$$

where χ_G is chosen for numerical integration criteria, because the $(1 - \varepsilon_j^2)$ term in Eq. [18.4] imposes an empirical thermodynamic constraint as ε_j approaches 1.

Once again, the motivation for Eq. (18.4) is based on minimizing the number of free parameters. Since ν_j and κ_j have predetermined values for all reactions [45], except for reaction $r_{1,4}$ discussed below, reaction rates solely depend on the values of the optimal control variables and the concentration of the state variables.

A process that is difficult to model is biofilm formation in the MCs. After several hundred days of operation, considerable biomass accumulated on the reactor walls, even though the MCs were gently mixed. While we could have developed a sophisticated biofilm sub-model, this would result in numerous poorly defined additional parameters. Instead, we simply introduce one parameter, f_{PL}, to represent the fraction of particulate matter (both living and detrital) that is not subject to chemostat washout because it is associated with the biofilm (see Table A.1).

18.3.3 Optimization Model

To determine how ε_j and $\omega_{i,j}$ must vary over time in order to maximize internal entropy production, we formulate and solve a receding horizon optimal control (RHOC) problem [7, 30]. RHOC is used in many fields. For example, in economics RHOC is used to determine how short-term investments should be allocated to maximize long-term returns, such as in retirement fund management. Because long-term prediction of markets is not perfect, short-term strategies are updated periodically based on current mark conditions. We implement a similar approach and maximize internal entropy production over successive intervals of time as given by,

$$\max_{\mathbf{u}(t_{n+1})} \frac{1}{\Delta t^*} \int_{t_n}^{t_n + \Delta t^*} \dot{\sigma}(\tau) e^{-k_w(\tau - t_n)} d\tau \quad \textit{where} \quad \mathbf{u} = \left[\boldsymbol{\varepsilon}^T \; \boldsymbol{\omega}^T \right]^T \tag{18.6a}$$

$$\textit{subject to}: \quad \frac{d\mathbf{x}(t)}{dt} = \mathbf{f}(\mathbf{x}(t), \mathbf{u}(t)) \quad \textit{and} \quad \mathbf{0} < \mathbf{u}(t) \le \mathbf{1} \tag{18.6b}$$

UNCORRECTED PROOF

Layout: T1 Standard SC | Book ID: 272293_1_En | Book ISBN: 978-3-642-40153-4
Chapter No.: 18 | Date: 17-8-2013 | Page: 11/23

Author Proof

where Δt^* is the long-term optimization interval from the current time, t_n, over which entropy production, $\dot{\sigma}$, is maximized. A conventional weighting function, $e^{-k_w(t-t_n)}$, discounts the importance of entropy production as time increases beyond t_n due to uncertainties in predicting future states. After the value of the optimal control variables ε_j and $\omega_{i,j}$, are determined over the optimization interval $[t_n,\ t_n + \Delta t^*]$, the state equations are updated only to $t_{n+1} = t_n + \Delta t$, where $\Delta t \leq \Delta t^*$, as illustrated in Fig. 18.1. The updating interval, Δt, is typically less than Δt^* to minimize discontinuities in state and control variables at the end of an interval. Average internal entropy production over the update interval, Δt, is given by,

$$\langle \dot{\sigma}(t_{n+1}) \rangle = \frac{1}{\Delta t} \int_{t_n}^{t_n+\Delta t} \dot{\sigma}(\tau) d\tau. \tag{18.7}$$

Total internal entropy produced over k intervals is given by $\sigma(t_n : t_{n+k}) = \Delta t \sum_{i=1}^{k} \langle \dot{\sigma}(t_{n+i}) \rangle$. Once the state and control variables are updated to $t_{n+1} = t_n + \Delta t$, Eq. (18.6a) is used to solve the next optimization interval, $t_{n+1} + \Delta t^*$ to extend the solution to $t_{n+2} = t_{n+1} + \Delta t$; this iteration is repeated until the desired final simulation time is reached.

The optimization, Eq. (18.6a), is subject to box constraints on the control variables between 0 and 1, and by mass balance constraints on the state variables, $\mathbf{x}(t)$, given by the differential equations defined by $\mathbf{f}(\mathbf{x}(t), \mathbf{u}(t))$ in Eq. (18.6b). The state variables for the microcosm experiment consist of nutrient concentrations, $\mathbf{c}(t)$, gas partial pressures, $\mathbf{p}(t)$, and concentration of biological structures, $\mathbf{c}_S(t)$, so that $\mathbf{x}(t) = \left[\mathbf{c}^T(t), \mathbf{p}^T(t), \mathbf{c}_S^T(t)\right]^T$. The mass balance equations are listed in the Appendix (Table A.1). The differential equations were numerically integrated using a high precision method [6] and the optimization problem was solved using a derivative free algorithm (BOBYQA [39]). Control variables are discretized over the $[t_n,\ t_n + \Delta t^*]$ interval using n_{knots} grid points and linear interpolation is used to produce continuous control functions.

18.4 Results

Time zero of the microcosm experiments corresponds to 00:00 20 Aug 2010, and on day 210.5 gas cycling of microcosms (MC) 1 and 4 commenced after experimental operating conditions had been finalized, in particular nitrogen-limited growth was achieved. Numerical simulations using the MaxEP-based BGC model were initialized on day 100, which provided sufficient time to achieve steady state conditions prior to gas cycling. Both experimental and modeling results are compared over days 200–500.

UNCORRECTED PROOF

Layout: T1 Standard SC | Book ID: 272293_1_En | Book ISBN: 978-3-642-40153-4
Chapter No.: 18 | Date: 17-8-2013 | Page: 12/23

Author Proof
B & W IN PRINT

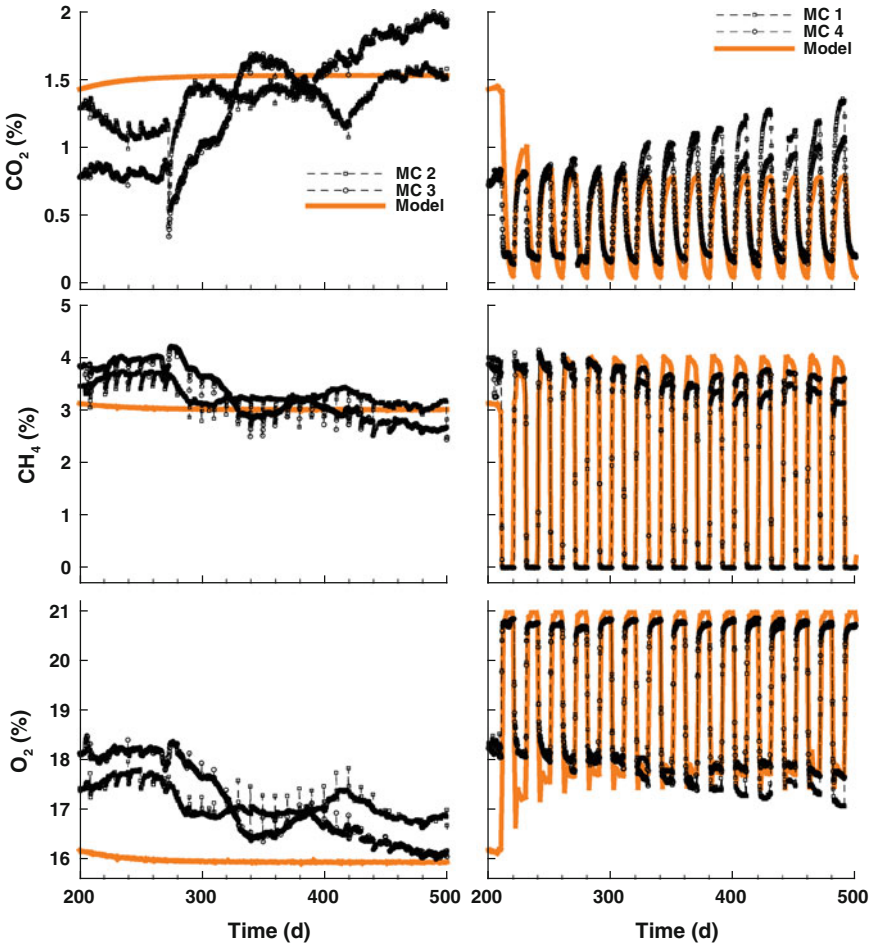

Fig. 18.3 Observed and modeled reactor exit gas concentrations for the controls (MC 2 and 3, *left column*) and cycled (MC 1 and 4, *right column*) microcosms. Modeled predictions are shown as the *orange* (or *grey* in BW) *solid line*, while experimental data are shown as open symbols connected by *dashed lines*. Model results are for $k_w = 0.230$ d^{-1}, $\Delta t = 10$ d and $\Delta t^* = 20$ d

Only two model parameters were qualitatively adjusted to achieve reasonable agreement between model results and observations for all four MCs (Figs. 18.3 and 18.4). Because detritus is a rather amorphous, non-polymeric material, its decomposition is difficult and is often the rate limiting step in microbial BGC [14]. Consequently, we reduced v_4 in Eq. (18.4) to 35 d^{-1} from the standard value of 350 d^{-1} [45]. We also tuned the biofilm parameter, f_{PL}, to 0.2. All other parameter values are well-defined constants, such as MC volume, dilution rate, feed concentrations, etc. All model degrees of freedom, other than v_4 and f_{PL}, reside in

Layout: T1 Standard SC | Book ID: 272293_1_En | Book ISBN: 978-3-642-40153-4
Chapter No.: 18 | Date: 17-8-2013 | Page: 13/23

Author Proof
B & W IN PRINT

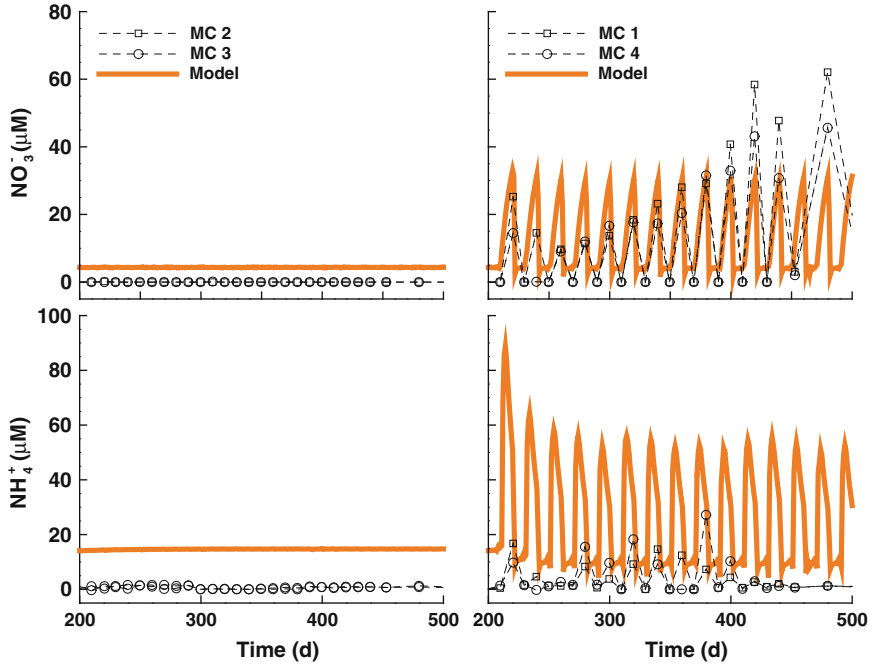

Fig. 18.4 Simulated data [*orange* (or *grey*) *lines*] compared to observations of nitrate and ammonium concentrations for the control MCs (MC 2 and 3, *left column*) and the methane cycled MCs (MC 1 and 4, *right column*). Also see caption to Fig. 18.3

Table 18.2 Internal entropy produced over 400 days for the control and gas-cycled simulations for different optimal interval parameters values: k_w, Δt and Δt^*

Δt	Δt^*	k_w	n_{knots}	$\sigma(100:500)$ (kJ K^{-1})	
(d)	(d)	(d^{-1})		Control	Cycled
0.1	0.1	0	1	2.07	1.45
0.1	1	3.00	5	18.56	7.71
1	1	0	1	16.82	6.94
1	5	0.921	5	22.85	9.05
10	20	0.230	15	24.19	10.53
20	40	0.115	20	24.64	14.55
20	50	0.0921	25	24.77	15.15

the 6 optimal control variables and the three interval optimization parameters, k_w, Δt and Δt^*.

To examine how the optimal interval parameters affect the solution and overall internal entropy production, we conducted several simulations by varying k_w, Δt and Δt^* for both the control and the gas-cycled simulations (Table 18.2). In general, these results show that as the optimization interval increases, total

Layout: T1 Standard SC | Book ID: 272293_1_En | Book ISBN: 978-3-642-40153-4
Chapter No.: 18 | Date: 17-8-2013 | Page: 14/23

Author Proof

internal entropy produced (σ) over the 400 days of simulation increases, but asymptotes to approximately 25 and 15 kJ K^{-1} for the control and gas-cycled simulations, respectively. Except for very short intervals, entropy production in the control simulations is not strongly affected by choices of Δt or Δt^* (Table 18.2). However, for very short optimization intervals ($\Delta t^* = 0.1$ d), entropy production is significantly depressed (Table 18.2). A similar phenomenon occurs in the gas-cycled simulations, but the decrease in total entropy production as Δt^* decreases is more gradual.

As Δt^* becomes small, biological structures are allocated to maximize entropy production in a manner that resembles abiotic systems, such as fire. In particular, examination of the control simulations reveals that the system does not sufficiently allocate resources to biological structure turnover, $\mathbb{S}_3$. The concentration of $\mathbb{S}_3$ in the control simulation with $\Delta t^* = 0.1$ is approximately equal to $\mathbb{S}_1$ and $\mathbb{S}_2$, but in the simulation with larger Δt^* values, $\mathbb{S}_3$ concentration is twice that of $\mathbb{S}_1$ and $\mathbb{S}_2$. The optimal controller attains higher concentration of $\mathbb{S}_3$ by setting ε_3 to approximately 0.62, while in the low entropy producing case ε_3 is only set to 0.34. The higher concentration of $\mathbb{S}_3$ allows the system to achieve much higher remineralization rates, so that reactions $r_{2,1}$ and $r_{2,2}$ can attain much higher rates due to the increase in NH_3 availability from $\mathbb{S}_i$ turnover. However, under short optimization intervals, the system's time horizon is too short to realize a return on investment in $\mathbb{S}_3$ with respect to entropy production or utilization of available chemical potential. When the time scale is short, the system does not make best use of available resources.

The gas-cycled simulations also generate interesting results when different $(\Delta t, \Delta t^*)$ values are examined. Figure 18.5a shows methanol dynamics over two gas cycling periods (40 d, beginning on day 300) for four selected simulations in Table 18.2 based on the $(\Delta t, \Delta t^*)$ values. When time scales are short, $(\Delta t, \Delta t^*) = (0.1, 1$ d) and (1, 5 d), methanol (CH_3OH) accumulates immediately after methane gas is turned on (at 300.5 and 320.5 d; Fig. 18.5a, dashed lines). However, when the time scale specified by the optimization parameters approach the period length of the gas cycling, $(\Delta t, \Delta t^*) = (10,\ 20$ d) and (20, 50 d), methanol accumulation occurs immediately before methane is switched off (at 310.5 and 330.5 days; Fig. 18.5a, solid lines). When the optimization time scales are long, the model develops an anticipatory control strategy, where methanol is produced as a storage compound that can be utilized during the phase when methane is absent. By storing some of the methane captured in the first half of the cycle as methanol, the system is able to oxidize more methane and produce more internal entropy compared to the simulations using short term optimization parameters. The strategy only accumulates methanol near the end of the period, because methanol is also lost due to dilution, which does not contribute to internal entropy production.

We can see how the control strategy achieves methanol accumulation by examining the concentration of biological structures and growth efficiencies for the case where $(\Delta t, \Delta t^*)$ equals (20, 50 d) over the two gas cycling periods

UNCORRECTED PROOF

Layout: T1 Standard SC | Book ID: 272293_1_En | Book ISBN: 978-3-642-40153-4
Chapter No.: 18 | Date: 17-8-2013 | Page: 15/23

Author Proof

B & W IN PRINT

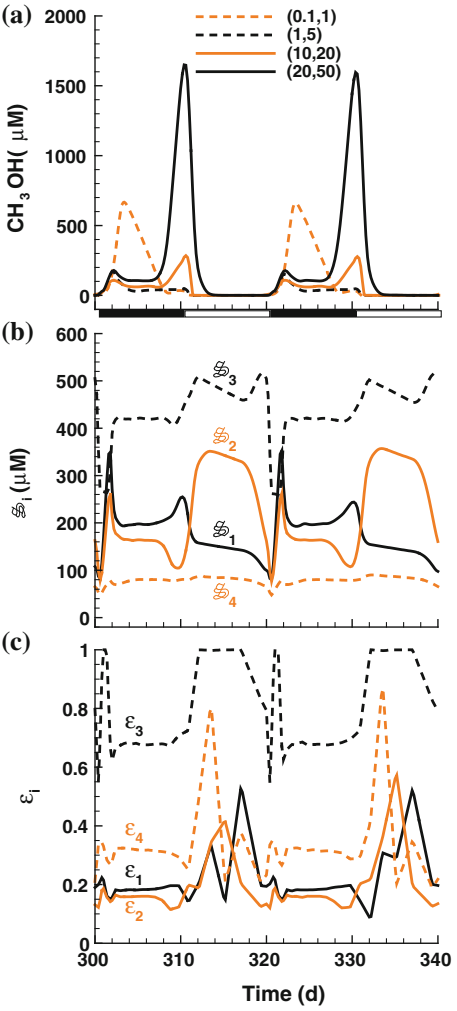

Fig. 18.5 (**a**) Methanol accumulation over two cycles for the optimization intervals given in the legend: $(\Delta t, \Delta t^*)$. The bar along the x axis shows when CH_4 gas is on (*black*) and off (*white*). Biological structures (**b**) and growth efficiencies (**c**) over two cycle periods for $(\Delta t, \Delta t^*) = (20\text{ d},\ 50\text{ d})$. All data are from the gas-cycled simulations only

(Fig. 18.5b, c). Just prior to the loss of methane (310.5 and 330.5 d), there is an increase in $\mathbb{S}_1$ and a decrease in $\mathbb{S}_2$ (Fig. 18.5b). Based on the reaction network (Fig. 18.2, Table 18.1), this allocation of catalyst favors methanol overproduction, so methanol accumulates rapidly. Immediately following the addition of methane, there is a rapid rise in $\mathbb{S}_2$ concentration and a decrease in $\mathbb{S}_1$, which drives methanol consumption up. To attain these changes in $\mathbb{S}_1$ and $\mathbb{S}_2$ abundances, there are the expected changes in the associated growth efficiencies (Fig. 18.5c), but there is also a large change in ε_3. In particular, ε_3 is driven to 1 following the loss of methane feed, which allows all biological structures to remain at high concentrations in the absence of methane because $r_{i,3}$ is driven to zero (Eq. 18.4). Just prior to the introduction of methane, ε_3 is reduced significantly, which causes

UNCORRECTED

Layout: T1 Standard SC | Book ID: 272293_1_En | Book ISBN: 978-3-642-40153-4
Chapter No.: 18 | Date: 17-8-2013 | Page: 16/23

Author Proof

a large turnover of biological structure (Fig. 18.5b), but biological structure concentrations quickly rebound once methane is again made available. To examine if these changes are occurring in the actual microcosms, we are currently sampling for cell abundances, DNA/RNA, and methanol concentration.

18.5 Discussion

In this chapter we have shown that a microbial biogeochemistry model based on the MaxEP principle produces results that are comparable to those obtained experimentally from microbial methanotrophic microcosms (Figs. 18.3 and 18.4). Unlike most microbial biogeochemistry models, the MaxEP model contains very few adjustable parameters, because we have been able to place most of the model's degrees of freedom into the optimal control variables, ε_j and $\omega_{i,j}$, whose values are determined by maximizing internal entropy production. By placing emphasis on catalytic activity at the system level, rather than on competition of individuals, the MaxEP approach provides a unique perspective on how ecosystems may function and evolve. Due to the novelty of the MaxEP approach, many of the ideas and conjectures that derive from MaxEP need to be tested, or at least shown to be improvements over canonical approaches. Microbial microcosms provide excellent experimental systems for testing MaxEP-based approaches for describing living systems, as microbial systems have fast characteristic times scales, high population densities and high biodiversity, all of which can be readily manipulated and monitored.

The MaxEP-BGC model predicts a comprehensive suite of output variables that can be compared to observations, only some of which were presented here. In addition to providing concentration data and reaction efficiencies, the model predicts reaction rates through the metabolic network (Table 18.1), reaction free energies, and how biological structure partitioning among sub-reactions changes over time (i.e., $\omega_{i,j}$). We expect our on-going measurements of community composition from 454-tag pyrosequencing and quantitative PCR analysis of function gene levels and expression will assist in comparing model output to observations [15]. Preliminary molecular results show that very high microbial diversity is maintained in the microcosms ($\sim$600 operational taxonomic units); however, community composition of the methanotrophs changes substantially over time (microscopic behavior), but this does not alter methane oxidation rates (macroscopic behavior), a characteristic consistent with MaxEP [9].

Perhaps the most intriguing result from our implementation of MaxEP for describing microbial biogeochemistry is the proposed distinction between abiotic and biotic systems based on instantaneous versus averaged entropy production. When entropy production is maximized instantaneously, no biological structure is produced because some of the free energy would simply be converted to another form of chemical potential instead of being destroyed. This problem is solved by

UNCORRECTED PROOF

Author Proof

maximizing entropy produced over an interval of time, which leads to the hypothesis. Because biotic systems are able to store information in their genome, they can implement temporal strategies that can out-compete abiotic processes in some situations. Because of genomic complexities, we do not know a priori the nature of the temporal strategies at this time, but this lack of knowledge can be circumvented by assuming that evolution has produced systems that extract the greatest possible free energy from a system over some appropriate characteristic time scale. Our results indicate (Table 18.2) that the longer the time scale, the more entropy that can be produced, but longer time scales require higher fidelity in predicting future states. Prediction in this case simply means that some of the temporal strategies the system possesses will be successful. Mismatches between prediction and the true state, due to perturbations, noise and uncertainties, ultimately limit the time scale interval for entropy production.

Our receding horizon optimal control implementation of the MaxEP problem shows that when time scales are short, biological structure should be invested for immediate entropy production, which leads to methanol production following the introduction of methane (Fig. 18.5a, dashed lines). This is an R-selection strategy [38], which is a possible driving mechanism for cross feeding [40], because partial substrate oxidation can increase growth rate [37]. When time scale is increased, the system allocates resources to $\mathbb{S}_3$ (the equivalent of grazers) as well as the later production of methanol that acts as a storage compound (Fig. 18.5a, solid lines). Systems oriented analyses of natural ecosystems indicate that the presence of grazers increases nutrient recycling and ecosystem productivity [31, 41, 42]. Predators, and trophic structures in general, increase the characteristic time scale of an ecosystem. It appears reasonable that organisms with long development times, or life histories, impart the long characteristic time scales observed in mature ecosystems, such as forests. Under this conjecture, bacterial systems may be closer to fire than an ecosystem composed of macroscopic organisms that provide the long characteristic time scale with respect to entropy production.

Experimentally, we expected more effective use of CH_4 in the gas-cycled treatment; that is, we expected entropy production to be similar between the control and gas-cycled MCs. Interestingly, the MaxEP-BGC model also has difficulties in producing entropy in the gas-cycled MCs (Table 18.2), but matches the experimental data well (Figs. 18.3 and 18.4). Because of methanol washout from the chemostat, the model only uses methanol as a storage compound near the end of the CH_4-on cycle, which limits the system's ability to store chemical potential. Storage of free energy in biological structure is also limited due to N requirements for $\mathbb{S}$. Perhaps the experiment and model are lacking higher trophic levels (i.e., macrofauna) that would provide a time scale relevant to the 20 day gas-cycle period. Currently, the model uses cannibalism of $\mathbb{S}_3$ as a means of trophic closure [33], so adding additional trophic levels may be one means of increasing the characteristic time scale in the model. As for the experiment, we are currently characterizing the eukaryotic community structure via cell counts.

Our MaxEP-BGC model currently focuses on microbes as reaction catalysts that dissipate chemical potential, but the MaxEP concept can be extended to macro-

UNCORRECTED PROOF

Layout: T1 Standard SC | Book ID: 272293_1_En | Book ISBN: 978-3-642-40153-4
Chapter No.: 18 | Date: 17-8-2013 | Page: 18/23

Author Proof

fauna and-flora as well. Metabolically, macroorganisms are rather prosaic; however, in addition to their longer characteristic time scales, they provide physical structure, increase the surface area of particulate matter via mastication and greatly enhance transport processes that often limit reaction rates [11, 18, 22]. Application of MaxEP to natural ecosystems will require understanding the functional contributions of macroorganisms, in particular with respect to transport processes, which is not a typical focus in ecology. More research needs to be done in this area.

18.6 Conclusions

We have been able to use the MaxEP conjecture to develop a microbial biogeochemistry model that reproduces reasonably well experimental data obtained from a methanotrophic microcosm experiment. By assuming that genomic information allows living systems to maximize entropy production over a characteristic time scale, we have been able to formulate the model as a receding horizon optimal control problem. Most of the model's degrees of freedom have been captured by the optimal control variables whose values are determined by maximizing entropy production over successive intervals of time. This approach greatly reduces the number of adjustable parameters whose values are often unknown, poorly constrained and seldom constant. Our results indicate that temporal strategies that are successful over greater durations of time will result in greater entropy production. From this hypothesis, we have developed a methanotrophic microcosm experiment to study how microbial communities respond, adapt and evolve to time varying inputs of energy. Based on experimental data to date, there appears to be good agreement between the MaxEP-BGC model results and experimental data.

All organisms possess genomic and acquired information that dictates survival strategies and life cycles that operate over defined characteristic time scales. These time scales can be as short as minutes or hours (i.e., for some bacteria) to as long as centuries or more (i.e., some tree species). Our approach has illustrated the importance that temporal strategies have on ecosystem dynamics, but our choice of time scale (for both Δt and Δt^*) has been somewhat arbitrary based on our intuitive understanding of bacterial growth and the reduced complexity of our experimental microcosms. Natural ecosystems are comprised of populations of different organisms that operate over a multitude of time scales. However, we hypothesize that organisms with long time scales can access more free energy (and ultimately producing more entropy) than those operating on short time scales provided the system is stable enough for long term predictions. Viewing ecosystems as a collection of free energy dissipating machines adaptively operating over a spectrum of time scales may help us understand how these systems assemble, operate and respond to disturbances of differing magnitude and frequency. Further research is needed relating the ecological concepts of temporal strategies and succession to quantitative measures and representations of time scales for the dissipation of free energy.

UNCORRECTED PROOF

Layout: T1 Standard SC | Book ID: 272293_1_En | Book ISBN: 978-3-642-40153-4
Chapter No.: 18 | Date: 17-8-2013 | Page: 19/23

Author Proof

578 **Acknowledgments** This research was supported by NSF grant EF-0928742 (Huber, Fernández
579 González, and Vallino), NSF grant OCE-1058747 (Algar, Vallino) and NSF grants CBET-
580 0756562, OCE-1058747 (Vallino). We thank Stefanie Strebel for sample analyses and assistance
581 in operation of the microcosms.

AQ1

582 # Appendix

583 Tables A.1 and A.2.

Table A.1 Mass balance equations for the rates of change of chemical species concentrations in the microcosm model used for constraints in Eq. (18.6b)*

$$\dot{c}_{CH_4}(t) = -r_{1,1} - r_{2,1} + \Big(F_L(c^f_{CH_4} - c_{CH_4}) + k_L a(p_{CH_4}/k_{CH_4}(T) - c_{CH_4})\Big)/V_L$$

$$\dot{c}_{CH_3OH}(t) = (1-\varepsilon_1)(r_{1,1} + r_{2,1}) - r_{1,2} - r_{2,2} + \Big(F_L(c^f_{CH_3OH} - c_{CH_3OH}) + k_L a(p_{CH_3OH}/k_{CH_3OH}(T) - c_{CH_3OH})\Big)/V_L$$

$$\dot{c}_{H_2CO_3}(t) = (1-\varepsilon_2)(r_{1,2} + r_{2,2}) + \varepsilon_3(1-\varepsilon_3)\sum_{i=1}^{4} r_{i,3} + (1-\varepsilon_4)r_{1,4} + \Big(F_L(c^f_{H_2CO_3} - c_{H_2CO_3}) + k_L a(p_{CO_2}/k_{H_2CO_3}(T) - c_{H_2CO_3})\Big)/V_L$$

$$\dot{c}_{dC}(t) = (1-\varepsilon_3)^2 \sum_{i=1}^{4} r_{i,3} - r_{1,4} + F_L(c^f_{dC} - f_{PL}c_{dC})/V_L$$

$$\dot{c}_{HNO_3}(t) = -\varepsilon_1\gamma_1 r_{1,1} - \varepsilon_2\gamma_2 r_{1,2} + F_L(c^f_{HNO_3} - c_{HNO_3})/V_L$$

$$\dot{c}_{NH_3}(t) = -\varepsilon_1\gamma_1 r_{2,1} - \varepsilon_2\gamma_2 r_{2,2} + \varepsilon_3 \sum_{i=1}^{4}((2-\varepsilon_3)\gamma_i - \gamma_3)\, r_{i,3} + d_{1,4}r_{1,4} + F_L(c^f_{NH_3} - c_{NH_3})/V_L$$

$$\dot{c}_{dN}(t) = (1-\varepsilon_3)^2 \sum_{i=1}^{4} \gamma_i r_{i,3} - \gamma_{dCN} r_{1,4} + F_L(c^f_{dN} - f_{PL}c_{dN})/V_L$$

$$\dot{c}_{O_2}(t) = -\sum_{i=1}^{2}\sum_{j=1}^{2} a_{i,j} r_{i,j} - \sum_{i=1}^{4} a_{i,3} r_{i,3} - a_{1,4} r_{1,4} + \Big(F_L(c^f_{O_2} - c_{O_2}) + k_L a(p_{O_2}/k_{O_2}(T) - c_{O_2})\Big)/V_L$$

$$\dot{p}_{CH_4}(t) = \Big(F_G(p^f_{CH_4} - p_{CH_4}) + k_L a\, RT(c_{CH_4} - p_{CH_4}/k_{CH_4}(T))\Big)/V_G$$

$$\dot{p}_{CH_3OH}(t) = \Big(F_G(p^f_{CH_3OH} - p_{CH_3OH}) + k_L a\, RT(c_{CH_3OH} - p_{CH_3OH}/k_{CH_3OH}(T))\Big)/V_G$$

$$\dot{p}_{CO_2}(t) = \Big(F_G(p^f_{CO_2} - p_{CO_2}) + k_L a\, RT(c_{H_2CO_3} - p_{CO_2}/k_{H_2CO_3}(T))\Big)/V_G$$

$$\dot{p}_{O_2}(t) = \Big(F_G(p^f_{O_2} - p_{O_2}) + k_L a\, RT(c_{O_2} - p_{O_2}/k_{O_2}(T))\Big)/V_G$$

$$\dot{c}_{S_j}(t) = \varepsilon_j \sum_{i=1}^{n_{S_j}} r_{i,j} - r_{j,3} + F_L(c^f_{S_j} - f_{PL}c_{S_j})/V_L \quad \text{for } j = 1,\ldots,4$$

*The superscript f refers to concentration of variables in the feed stream, F_L and F_G are the liquid and gas volumetric feed rates, respectively, $k_L a$ is the liquid-side mass transfer coefficient, $k_h(T)$ is a Henry's law coefficient for solute h, V_G is the gas headspace volume, and f_{PL} is the fraction of particulate matter loss due to dilution; that is, not associated with the biofilm

UNCORRECTED PROOF

Layout: T1 Standard SC | Book ID: 272293_1_En | Book ISBN: 978-3-642-40153-4
Chapter No.: 18 | Date: 17-8-2013 | Page: 20/23

Author Proof

Table A.2 Nomenclature

Variable	Definition	Units
$a_{i,j}$	Oxygen stoichiometric coefficient for reaction $r_{i,j}$ (see Table 18.1)	
$b_{i,j}$	Water stoichiometric coefficient for reaction $r_{i,j}$ (see Table 18.1)	
c_i	Concentration of species i (**c** in vector form)	mmol m^{-3}
c_i^f	Concentration of species i in microcosm feed	mmol m^{-3}
c_{S_j}	Concentration of biological structure j	mmol m^{-3}
$d_{i,j}$	Ammonia stoichiometric coefficient for reaction $r_{i,j}$ (see Table 18.1)	
dC	Detrital organic carbon	
dN	Detrital organic nitrogen	
f_{PL}	Fraction of particulate matter loss due to dilution	
f	Vector function of state equations (see Table A1)	
$k_i(T)$	Henry's law coefficient for solute i	Pa m^3 $mmol^{-1}$
k_La	Air–water gas transfer coefficient, liquid side	m^3 d^{-1}
k_w	Optimization discounting parameter	d^{-1}
n_c	Number of chemical species	
n_{knots}	Number of grid points for discretizing control variables over an optimization interval (see Table 18.2)	
n_S	Number of biological structures, $\mathbb{S}_j$	
n_{S_j}	Number of sub-reactions associated with $\mathbb{S}_j$	
p_i	Partial pressure of gas species i	Pa
p_i^f	Partial pressure of gas species i in feed gas	Pa
$r_{i,j}$	Reaction rate	mmol m^{-3} d^{-1}
Δt	Optimization update interval	d
Δt^*	Optimization interval	d
t	Time	d
u	Vector of control variables ($\boldsymbol{\varepsilon}$, $\boldsymbol{\omega}$)	
x	Vector of state variables (**c**, **p**, $\mathbf{c}_S$)	
F_G	Gas flow rate to microcosms	m^3 d^{-1}
F_L	Liquid flow rate to microcosms	m^3 d^{-1}
$\Delta_r G_{r_{i,j}}$	Gibbs free energy of reaction for reaction $r_{i,j}$	kJ $mmol^{-1}$
R	Gas constant (units depend on equation)	
S	System entropy	kJ K^{-1}
$\mathbb{S}_j$	Biological structure j that catalyzes reaction $r_{i,j}$	
T	Temperature	K
V_G	Gas volume of microcosm	m^{-3}
V_L	Liquid volume of microcosm	m^{-3}
α_i	Hydrogen atoms in unit carbon formula for biological structure i	
β_i	Oxygen atoms in unit carbon formula for biological structure i	
γ_i	Nitrogen atoms in unit carbon formula for biological structure i	
ε_j	Growth efficiency for biological structure j. (Optimal control variable)	
κ_j	Substrate affinity parameter in reaction $r_{i,j}$	mmol m^{-3}
v_j	Maximum specific reaction rate for reaction $r_{i,j}$	d^{-1}
σ	Entropy produced from irreversible processes within system	kJ K^{-1}
$\dot{\sigma}$	Rate of internal entropy production	kJ K^{-1} d^{-1}
χ_G	Parameter in free energy weighting function, f_G	mmol kJ^{-1}

(continued)

UNCORRECTED PROOF

Author Proof

Table A.2 (continued)

Variable	Definition	Units
$\omega_{i,j}$	Partition coef. of biological structure j to sub-reaction $r_{i,j}$. (Optimal control variable)	
$\Lambda_{i,j,k}$	Stoichiometric exponent for reaction $r_{i,j}$ for c_k	
$\langle\rangle$	Expectation operator	

References

1. Adami, C.: Information theory in molecular biology. Phys. Life Rev. **1**(1), 3–22 (2004). doi:10.1016/j.plrev.2004.01.002
2. Alberty, R.A.: Thermodynamics of biochemical reactions. Wiley, Hoboken (2003)
3. Battley, E.: Absorbed heat and heat of formation of dried microbial biomass: studies on the thermodynamics of microbial growth. J. Therm. Anal. Calorim. **74**(3), 709–721 (2003). doi:10.1023/B:JTAN.0000011003.43875.0d
4. Battley, E.H.: The development of direct and indirect methods for the study of the thermodynamics of microbial growth. Thermochim. Acta **309**(1–2), 17–37 (1998)
5. Berut, A., Arakelyan, A., Petrosyan, A., Ciliberto, S., Dillenschneider, R., Lutz, E.: Experimental verification of Landauer/'s principle linking information and thermodynamics. Nature **483**(7388), 187–189 (2012). doi:10.1038/nature10872
6. Brugnano, L., Magherini, C.: The BiM code for the numerical solution of ODEs. J. Comput. Appl. Math. **164–165**, 145–158 (2004). doi:10.1016/j.cam.2003.09.004
7. Chen, H., Allgower, F.: A quasi-infinite horizon nonlinear model predictive control scheme with guaranteed stability. Automatica **34**(10), 1205–1217 (1998). doi:10.1016/S0005-1098(98)00073-9
8. Dewar, R.: Information theory explanation of the fluctuation theorem, maximum entropy production and self-organized criticality in non-equilibrium stationary states. J. Phys. A: Math. Gen. **36**, 631–641 (2003)
9. Dewar, R.: Maximum entropy production as an inference algorithm that translates physical assumptions into macroscopic predictions: don't shoot the messenger. Entropy **11**(4), 931–944 (2009). doi:10.3390/e11040931
10. Dewar, R.C.: Maximum entropy production and the fluctuation theorem. J. Phys. A: Math. Gen. **38**(21), L371–L381 (2005). doi:10.1088/0305-4470/38/21/L01
11. Erwin, D.H.: Macroevolution of ecosystem engineering, niche construction and diversity. Trends Ecol. Evol. **23**(6), 304–310 (2008). doi:10.1016/j.tree.2008.01.013
12. Falkowski, P.G., Fenchel, T., DeLong, E.F.: The microbial engines that drive earth's biogeochemical cycles. Science **320**(5879), 1034–1039 (2008). doi:10.1126/science.1153213
13. Friedrichs, M.A.M., Dusenberry, J.A., Anderson, L.A., Armstrong, R.A., Chai, F., Christian, J.R., Doney, S.C., Dunne, J., Fujii, M., Hood, R., McGillicuddy, D.J., Jr., Moore, J.K., Schartau, M., Spitz, Y.H., Wiggert, J.D (2007) Assessment of skill and portability in regional marine biogeochemical models: Role of multiple planktonic groups. J.Geophys.Res. **112**(C8), C08001
14. Horner, J.D., Gosz, J.R., Cates, R.G.: The role of carbon-based plant secondary metabolites in decomposition in terrestrial ecosystems. Am. Nat. **132**(6), 869–883 (1988)
15. Huber, J.A., Cantin, H.V., Huse, S.M., Mark Welch, D.B., Sogin, M.L., Butterfield, D.A (2010) Isolated communities of Epsilonproteobacteria in hydrothermal vent fluids of the Mariana Arc seamounts. FEMS Microbiology Ecology **73**(3), 538–549. doi:10.1111/j.1574-6941.2010.00910.x

UNCORRECTED PROOF

Layout: T1 Standard SC | Book ID: 272293_1_En | Book ISBN: 978-3-642-40153-4
Chapter No.: 18 | Date: 17-8-2013 | Page: 22/23

Author Proof

16. Huber, J.A., Welch, D.B.M., Morrison, H.G., Huse, S.M., Neal, P.R., Butterfield, D.A., Sogin, M.L.: Microbial population structures in the deep marine biosphere. Science **318**(5847), 97–100 (2007). doi:10.1126/science.1146689
17. Jaynes, E.T.: The Gibbs paradox. In: Smith, C.R., Erickson, G.J., Neudorfer, P.O. (eds.) Maximum entropy and Bayesian methods, pp. 1–22. Kluwer Academic Publisheres, Dordrecht (1992)
18. Jones, C.G., Lawton, J.H., Shachak, M.: Organisms as ecosystem engineers. Oikos **69**(3), 373–386 (1994)
19. Kleidon, A., Fraedrich, K., Kunz, T., Lunkeit, F.: The atmospheric circulation and states of maximum entropy production. Geophys. Res. Lett. **30**(23), 1–4 (2003). doi:10.1029/2003GL018363
20. Kondepudi, D., Prigogine, I.: Modern thermodynamics: from heat engines to dissipative structures. Wiley, New York (1998)
21. Kuenen, J.G.: Anammox bacteria: from discovery to application. Nat. Rev. Micro. **6**(4), 320–326 (2008). doi:10.1038/nrmicro1857
22. Lawton, J.H.: What do species do in ecosystems? Oikos **71**(3), 367–374 (1994)
23. Lennon, J.T., Jones, S.E.: Microbial seed banks: the ecological and evolutionary implications of dormancy. Nat. Rev. Micro. **9**(2), 119–130 (2011). doi:10.1038/nrmicro2504
24. Lewis, K.: Persister cells. Annu. Rev. Microbiol. **64**(1), 357–372 (2010). doi:10.1146/annurev.micro.112408.134306
25. Lineweaver, C.H., Egan, C.A.: Life, gravity and the second law of thermodynamics. Physics of Life Reviews **5**(4), 225–242 (2008). doi:10.1016/j.plrev.2008.08.002
26. Lorenz, R.: Computational mathematics: full steam ahead-probably. Science **299**(5608), 837–838 (2003)
27. Lorenz, R.D., Lunine, J.I., Withers, P.G.: Titan, mars and earth: entropy production by latitudinal heat transport. Geophys. Res. Lett. **28**(3), 415–418 (2001)
28. Makela, T., Annila, A.: Natural patterns of energy dispersal. Phys. Life Rev. **7**(4), 477–498 (2010). doi:10.1016/j.plrev.2010.10.001
29. Martyushev, L.: Some interesting consequences of the maximum entropy production principle. J. Exp. Theor. Phys. **104**(4), 651–654 (2007). doi:10.1134/S1063776107040152
30. Mayne, D.Q., Rawlings, J.B., Rao, C.V., Scokaert, P.O.M.: Constrained model predictive control: Stability and optimality. Automatica **36**(6), 789–814 (2000). doi:10.1016/S0005-1098(99)00214-9
31. Mazancourt, D.C., Loreau, M.: Grazing optimization, nutrient cycling, and spatial heterogeneity of plant-herbivore interactions: should a palatable plant evolve? Evolution **54**(1), 81–92 (2000)
32. Meysman, F.J.R., Bruers, S.: A thermodynamic perspective on food webs: quantifying entropy production within detrital-based ecosystems. J. Theor. Biol. **249**(1), 124–139 (2007). doi:10.1016/j.jtbi.2007.07.015
33. Mitra, A.: Are closure terms appropriate or necessary descriptors of zooplankton loss in nutrient-phytoplankton-zooplankton type models? Ecol. Model. **220**(5), 611–620 (2009). doi:10.1016/j.ecolmodel.2008.12.008
34. Morrison, P.: A thermodynamic characterization of self-reproduction. Rev. Mod. Phys. **36**(2), 517 (1964)
35. Niven, R.K.: Steady state of a dissipative flow-controlled system and the maximum entropy production principle. Physical review E (Statistical, Nonlinear, and Soft Matter Physics) **80**(2), 021113–021115. (2009) doi:10.1103/PhysRevE.80.021113
36. Paltridge, G.W.: Global dynamics and climate-a system of minimum entropy exchange. Q. J. Roy. Met. Soc. **104**, 927–945 (1975)
37. Pfeiffer, T., Bonhoeffer, S.: Evolution of cross-feeding in microbial populations. Am. Nat. **163**(6), E126–E135 (2004)
38. Pianka, E.R.: R-selection and K-selection. Am. Nat. **104**(940), 592–597 (1970)
39. Powell, M.J.D.: The BOBYQA algorithm for bound constrained optimization without derivatives. Optim. Online **5**, 1–39 (2010)

UNCORRECTED PROOF

Layout: T1 Standard SC | Book ID: 272293_1_En | Book ISBN: 978-3-642-40153-4
Chapter No.: 18 | Date: 17-8-2013 | Page: 23/23

Author Proof

40. Rosenzweig, R.F., Sharp, R.R., Treves, D.S., Adams, J.: Microbial evolution in a simple unstructured environment: genetic differentiation in escherichia coli. Genetics **137**(4), 903–917 (1994)
41. Schmitz, O.J., Hawlena, D., Trussell, G.C.: Predator control of ecosystem nutrient dynamics. Ecol. Lett. **13**(10), 1199–1209 (2010). doi:10.1111/j.1461-0248.2010.01511.x
42. Urabe, J., Elser, J.J., Kyle, M., Yoshida, T., Sekino, T., Kawabata, Z.: Herbivorous animals can mitigate unfavourable ratios of energy and material supplies by enhancing nutrient recycling. Ecol. Lett. **5**(2), 177–185 (2002). doi:10.1046/j.1461-0248.2002.00303.x
43. Vallino, J.J.: Modeling microbial consortiums as distributed metabolic networks. Biol. Bull. **204**(2), 174–179 (2003)
44. Vallino, J.J.: Ecosystem biogeochemistry considered as a distributed metabolic network ordered by maximum entropy production. Philos. Trans. Royal Soc. B: Biol. Sci. **365**(1545), 1417–1427 (2010). doi:10.1098/rstb.2009.0272
45. Vallino, J.J.: Differences and implications in biogeochemistry from maximizing entropy production locally versus globally. Earth Syst. Dynam. **2**(1), 69–85 (2011). doi:10.5194/esd-2-69-2011
46. Wang, J., Bras, R.L.: A model of evapotranspiration based on the theory of maximum entropy production. Water Resour. Res. **47**(3 (W03521)), 1–10 (2011) doi:10.1029/2010WR009392

UNCORRECTED PROOF